Intrinsic Motions in the N-Terminal Domain of an Ionotropic Glutamate Receptor Detected by Fluorescence Correlation Spectroscopy

ARTICLE *in* JOURNAL OF MOLECULAR BIOLOGY · NOVEMBER 2011

Impact Factor: 4.33 · DOI: 10.1016/j.jmb.2011.09.037 · Source: PubMed

5 AUTHORS, INCLUDING:

Ingo Greger
University of Cambridge
34 PUBLICATIONS **1,332** CITATIONS
SEE PROFILE

Hannes Neuweiler
University of Wuerzburg
40 PUBLICATIONS **1,248** CITATIONS
SEE PROFILE

doi:10.1016/j.jmb.2011.09.037 J. Mol. Biol. (2011) 414, 96–105

Contents lists available at www.sciencedirect.com

Journal of Molecular Biology

journal homepage: http://ees.elsevier.com.jmb

Intrinsic Motions in the N-Terminal Domain of an Ionotropic Glutamate Receptor Detected by Fluorescence Correlation Spectroscopy

Mette H. Jensen†, Madhav Sukumaran†, Christopher M. Johnson, Ingo H. Greger* and Hannes Neuweiler*

Medical Research Council Laboratory of Molecular Biology, Hills Road, Cambridge CB2 0QH, UK

Received 11 May 2011;
received in revised form
1 September 2011;
accepted 22 September 2011
Available online
6 October 2011

Edited by A. G. Palmer III

Keywords:
protein dynamics;
signaling;
single-molecule fluorescence;
fluorescence quenching

Ionotropic glutamate receptors (iGluRs) mediate excitatory neurotransmission in the central nervous system and play key roles in brain development and disease. iGluRs have two distinct extracellular domains, but the functional role of the distal N-terminal domain (NTD) is poorly understood. Crystal structures of the NTD from some non-*N*-methyl-D-aspartate (NMDA) iGluRs are consistent with a rigid body that facilitates receptor assembly but suggest an additional dynamic role that could modulate signaling. Here, we moved beyond spatial and temporal limitations of conventional protein single-molecule spectroscopy by employing correlation analysis of extrinsic oxazine fluorescence fluctuations. We observed nanosecond (ns)-to-microsecond (μs) motions of loop segments and helices within a region of an AMPA-type iGluR NTD, which has been identified previously to be structurally variable. Our data reveal that the AMPA receptor NTD undergoes rapid conformational fluctuations, suggesting an inherent allosteric capacity for this domain in addition to its established assembly function.

Introduction

Ionotropic glutamate receptors (iGluRs) are ligand-gated ion channels that are ubiquitously expressed in the central nervous system. These multi-domain tetrameric assemblies mediate signal transmission at excitatory synapses through binding of the chemical transmitter L-glutamate.[1] The receptors are involved in essentially all facets of nervous system development and function and are implicated in diseases involving neurodegenerative conditions and psychiatric disorders.[1,2] The four iGluR subfamilies [the α-amino-3-hydroxyl-5-methyl-4-isoxazole-propionate (AMPA) receptor (AMPAR), kainate receptor, delta receptor, and *N*-methyl-D-aspartate (NMDA) receptor] overall share a similar architecture with a single iGluR subunit comprising semi-independent domains: (i) the N-terminal domain (NTD) and (ii) the ligand-binding domain (LBD) that both face the extracellu-

**Corresponding authors.* H. Neuweiler is to be contacted at Department of Biotechnology and Biophysics, University of Würzburg, Am Hubland, 97074 Würzburg, Germany. E-mail addresses: ig@mrc-lmb.cam.ac.uk; hannes.neuweiler@uni-wuerzburg.de.

† M.H.J. and M.S. contributed equally to this work

Abbreviations used: ACF, autocorrelation function; AMPA, α-amino-3-hydroxyl-5-methyl-4-isoxazole-propionate; AMPAR, AMPA receptor; BSA, bovine serum albumin; FCS, fluorescence correlation spectroscopy; iGluR, ionotropic glutamate receptor; LBD, ligand-binding domain; NMDA, *N*-methyl-D-aspartate; NTD, N-terminal domain; OVA, ovalbumin; PDB, Protein Data Bank; PET, photoinduced electron transfer; TMD, transmembrane domain; LL, lower lobe; UL, upper lobe.

lar milieu and (iii) the transmembrane domain (TMD) that forms the ion channel (Fig. 1).

The structure and allosteric function of the LBD have been studied extensively,[1] where agonist binding induces conformational changes that are transmitted to the TMD, rapidly opening the channel pore and triggering receptor desensitization.[3,4] The C-terminal domain is involved in receptor localization.[5] In contrast, the function of the NTD is not established. To date, this most sequence diverse portion of the receptor has been associated mostly with receptor assembly[6] but may provide additional functions including transsynaptic protein–protein interactions, allosteric modulation of the ion channel, and transsynaptic signaling.[6–10] Both NTD and LBD are structurally related to the clamshell-shaped bacterial periplasmic-binding proteins, bilobate structures that capture ligands in their clamshell cleft.[11,12] Periplasmic-binding proteins are fused to a number of receptors in eukaryotes, where they are implicated in signal sensing and transmission.[13,14] Indeed, NTDs from the NMDA receptor subfamily harbor a binding site for allosteric modulators, rendering this domain a strategic drug target.[6,15–17] NTD ligands for the NMDA receptor have progressed into clinical trials.[18]

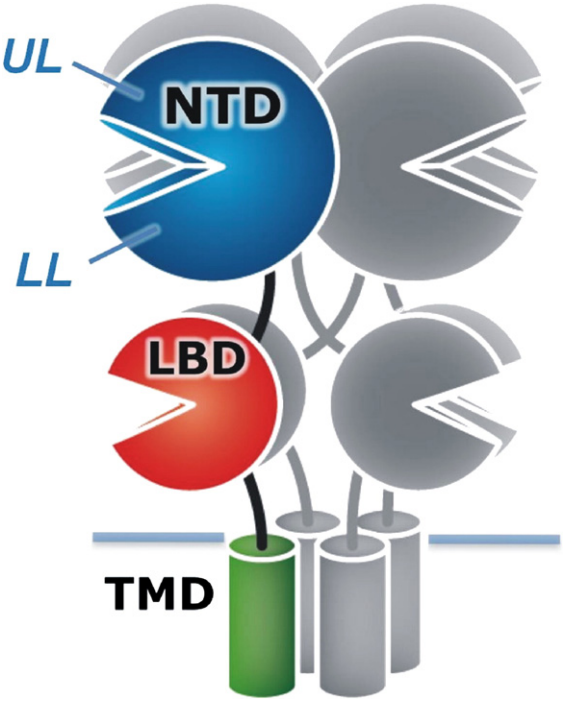

Fig. 1. Structural architecture of iGluRs. A receptor tetramer is shown. One single subunit of the tetrameric assembly contains three distinct semiautonomous domains that are connected by flexible polypeptide segments: the extracellular clamshell-shaped domains, that is, the NTD (blue), the LBD (red), and the TMD (green), which forms the ion channel. Upper and lower clamshell lobes of the NTD are indicated (UL and LL, respectively). The plane of the membrane is indicated by a horizontal line.

Purely based on the analysis of crystallographic data, a constrained rigid-body conformation has been suggested for AMPAR and kainate receptor NTDs.[9,10] Specifically, the dimeric packing across both the upper and the lower clamshell lobes has been interpreted to rule out protein chain mobility and signaling capacity, with modulation of subunit assembly proposed as the sole function of these NTDs.[9,10,19] However, recent crystallographic data analysis of GluA2 and GluA3 AMPA-type NTDs and computational normal mode analysis revealed structural heterogeneity in the lower lobes (LLs) and indicated intrinsic domain dynamics,[20] implying a currently unexplored allosteric capacity for AMPAR NTDs.

Protein dynamics are difficult to detect experimentally. Protein chain motions in native states are often fast (i.e., occur on the sub-millisecond timescale), and spectroscopic signatures are scant.[21] NMR spectroscopy is a powerful tool in investigating protein dynamics at atomic resolution. Modern NMR methods can resolve conformational motions on a broad range of timescales, provide fundamental insights into the dynamic nature of proteins, and elucidate the relation between protein dynamics and function.[21–23] However, NMR data analysis is becoming increasingly complicated for higher-molecular-weight species, and the method requires comparatively high protein sample concentrations that are not always feasible. Single-molecule spectroscopy, on the other hand, detects structural fluctuations that are hidden in the average signal from conventional bulk methods by monitoring fluorescence signals of individual, extrinsic labels introduced site-specifically into proteins, albeit not at atomic resolution. Single-molecule fluorescence data are recorded from highly dilute samples (typically, nanomolar concentrations and below), and the method tolerates complex sample mixtures that can approach the *in vivo* situation.[24] The nonradiative energy transfer from a donor fluorophore to an acceptor fluorophore, that is, fluorescence resonance energy transfer, probes global protein conformational changes on a scale of 2–10 nm,[24,25] but more local structural fluctuations remain hidden. Fluorescence quenching of extrinsic labels by the amino acid tryptophan (Trp) *via* photoinduced electron transfer (PET) occurs at van der Waals contact and probes structural changes around 1 nm. In combination with fluorescence correlation spectroscopy (FCS), the method is being used to detect kinetics of protein structural fluctuations at the level of individual molecules on timescales from nanoseconds (ns) to milliseconds (ms).[26–28]

Here, we used this technique to search for motions within the AMPAR GluA2 NTD. We identified site-specific sub-millisecond protein dynamics. Fluorescence quenching of an extrinsic label by an engineered

Trp residue uncovered a specific motion of helices in the LL of the NTD, in agreement with recent crystallographic data analysis, which showed structural variations.[20] The detected intra-lobe dynamics might be part of a previously hidden allosteric interaction network within the AMPAR NTD.

Results

FCS of protein dynamics

FCS analyzes fluorescence fluctuations arising from individual molecules diffusing through a minute (~1 fl = 10^{-15} l) detection volume by Brownian motion.[29,30] Fluorescence intensity time traces are recorded from molecular micro-ensembles (typically 10–50 molecules at a time) and processed to calculate the autocorrelation function (ACF). The ACF detects kinetics of virtually any process that gives rise to a fluctuation of fluorescence emission intensity. Besides molecular diffusion, protein dynamics that are faster than diffusion can be detected. The principle of the technique is illustrated in Fig. 2a. Extrinsic fluorophores introduced at specific sites within a protein can report changes in protein conformation by modulation of their fluorescence quantum yield. This modulation can occur through

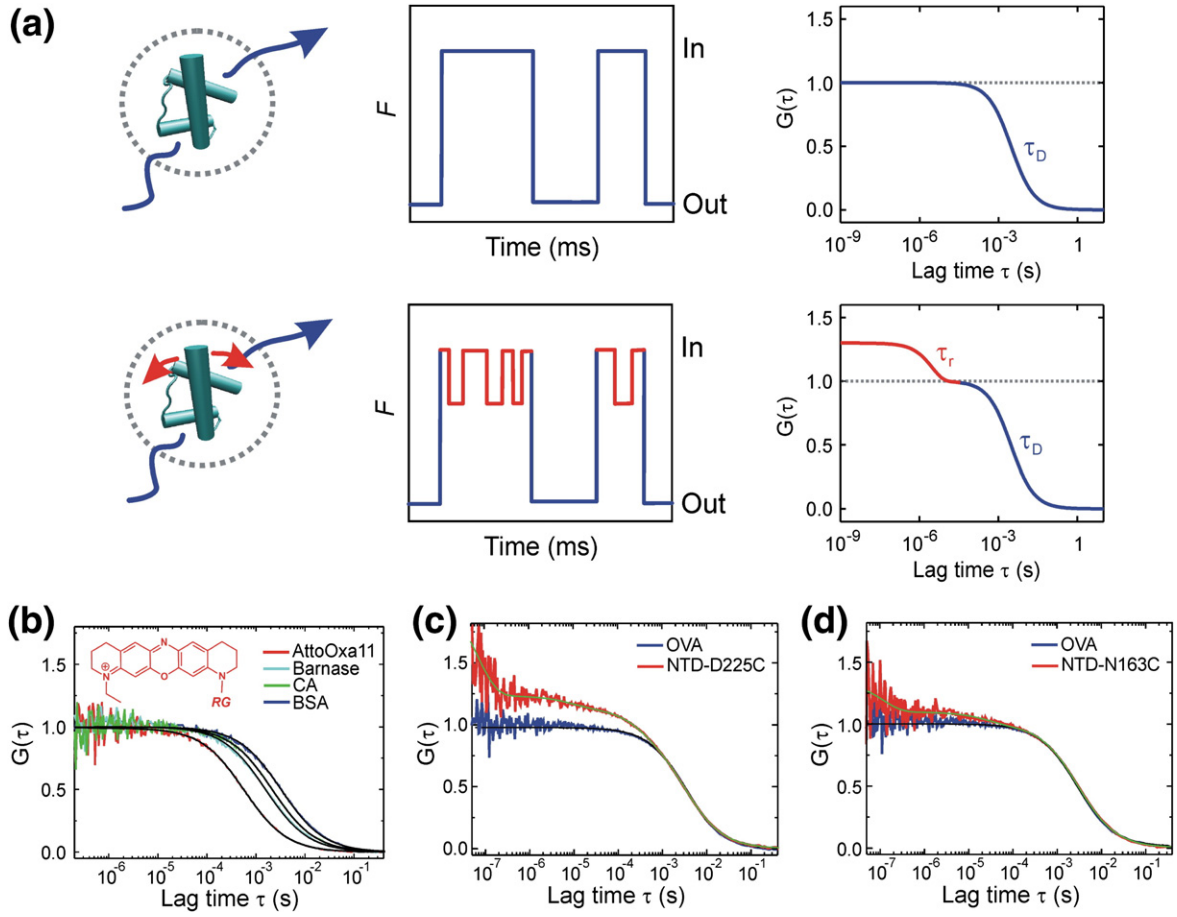

Fig. 2. FCS of protein dynamics. (a) Principle of measuring protein dynamics using FCS. Fluorescently modified proteins (cyan) diffuse through a confined detection volume (broken circle) by Brownian motion (blue lines) and cause stochastic fluctuations of fluorescence signals (*F*) at the detector. FCS analyses the temporal fluorescence fluctuations by calculating the ACF, G(τ), showing a decay with a characteristic time constant of diffusion, τ_D. If the protein exhibits intrinsic chain motions (red), which are faster than diffusion and which modulate fluorescence emission of the label, these motions are detected as additional decay of the ACF with a characteristic relaxation time constant, τ_r. (b) Recorded ACFs of rigid-body proteins. The chemical structure of the oxazine fluorophore (inset; RG, reactive group) and the corresponding ACF are also shown. Black lines are data fits to a model for a single monodisperse diffusion. (c and d) ACFs of fluorescently modified NTD mutants D225C and N163C. The green lines are data fits to a model for a single monodisperse diffusion plus three and two sub-millisecond single-exponential relaxations, respectively. The ACF of OVA, which has similar molecular mass to NTD and thus similar τ_D, fits well to a monodisperse diffusion without any additional fluctuations (black line). Each ACF shown is normalized to the fitted average number of detected molecules *N* for reasons of clarity (see Materials and Methods).

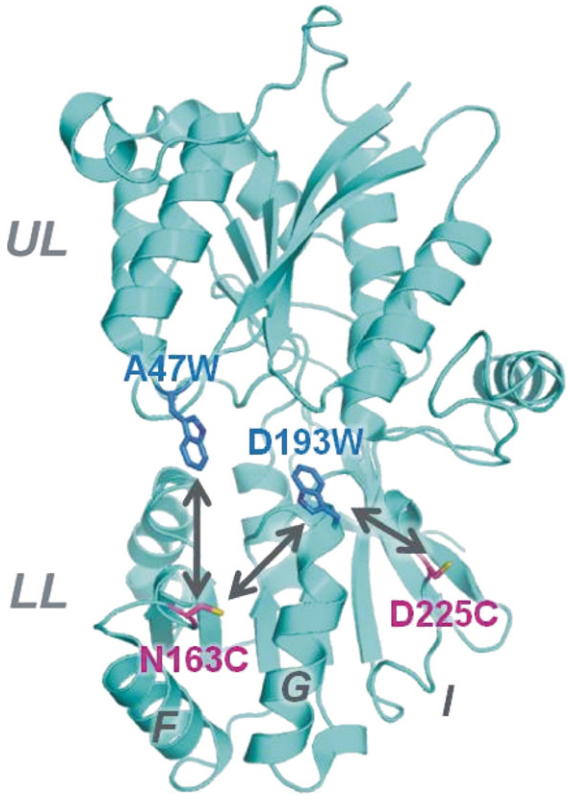

Fig. 3. Design of the fluorescence reporter system to detect NTD chain motions. View on the bilobed AMPAR GluA2 NTD (PDB ID 3HSY). UL and LL are indicated. Helices F and G and segment I in the LL are indicated. Cys side chains introduced for site-specific modification with the fluorophore are highlighted magenta. Individual Trp side chains introduced as PET fluorescence quencher are highlighted blue. Arrows indicate the coordinates of specific motions targeted by the reporter systems.

changes in polarity of the chromophore's microenvironment or through specific fluorescence-quenching interactions with nearby chemical moieties, such as engineered Trp side chains.[26,27,31]

Here, we first analyzed fluorescence fluctuations from a series of extrinsically modified globular rigid-body-type proteins to obtain baseline references. To this end, the proteins barnase, carbonic anhydrase, bovine serum albumin (BSA), and ovalbumin (OVA) were modified covalently with an oxazine fluorophore (Fig. 2b, inset). Oxazine fluorophores are advantageous for such studies because they lack photophysical fluorescence fluctuations at moderate excitation energies and facilitate the detection of protein chain motions at the single-molecule level with high signal-to-noise ratio.[28] The recorded ACFs fitted well to a model for a monodisperse molecular diffusion without any additional fluorescence fluctuations in the submillisecond time domain, in agreement with rigid-body globules (Fig. 2b).

Next, we introduced individual oxazine labels into the GluA2 AMPAR NTD; the reporter design is shown in Fig. 3. Individual cysteine (Cys) side chains were engineered as labeling positions by replacing the side chains of N163 in helix F and D225 in segment I, both of which are solvent exposed and are not involved in structural interactions, *via* mutagenesis. Cys side chains were then modified with a thiol-reactive derivative of the oxazine fluorophore (Fig. 2b, inset).

AMPAR NTDs contain two buried Cys side chains [C83 and C190; Protein Data Bank (PDB) ID 3HSY] and a disulfide bridge (C57–C309) in the upper lobe (UL) that could potentially be modified during the labeling reaction carried out under reductive conditions. The specificity of labeling was therefore tested by reacting wild-type protein under identical conditions. The lack of any detectable labeled wild-type NTD confirmed selective modification of engineered Cys side chains.

Prior to FCS experiments, stability of all NTD protein constructs was assessed by size-exclusion chromatography before and after labeling and verified by monodisperse (i.e., non-aggregating) elution profiles. The ACFs of NTD constructs D225C and N163C were dominated by molecular diffusion through the detection focus (Fig. 2c and d). The FCS diffusion time constant τ_D accurately reports protein size.[32] OVA and the AMPAR NTD are of similar molecular masses (43 kDa and ~46 kDa, respectively). Accordingly, the determined values of τ_D were similar (3.1 ± 0.2 ms and 3.3 ± 0.2 ms, respectively). However, for the NTD, additional fluorescence fluctuations in the sub-

Table 1. FCS kinetic parameter of GluA2 NTD

	N163C	N163C-A47W	N163C-D193W	D225C	D225C-D193W
τ_D (ms)	3.1 ± 0.1	3.6 ± 0.3	3.3 ± 0.1	3.1 ± 0.2	3.2 ± 0.1
a_1	0.09 ± 0.01	0.07 ± 0.03	0.12 ± 0.01	0.14 ± 0.04	0.14 ± 0.02
τ_1 (μs)	29 ± 8	51 ± 50	120 ± 20	300 ± 140	100 ± 30
a_2	—	—	0.11 ± 0.01	0.09 ± 0.02	0.15 ± 0.02
τ_2 (μs)	—	—	2.4 ± 0.5	9 ± 4	4 ± 1
a_3	0.26 ± 0.05	0.23 ± 0.03	0.77 ± 0.11	0.89 ± 0.14	0.59 ± 0.09
τ_3 (ns)	110 ± 30	510 ± 170	57 ± 6	67 ± 9	80 ± 10

Errors are standard errors of data fits.

millisecond time domain were apparent. This observation contrasted with rigid-body globules, which showed no such fluctuations (Fig. 2b–d). The overall amplitude of the relaxation was significantly higher for C225 in segment I compared to C163 in helix F. The relaxations were best described by a model containing a sum of three and two single-exponential decay functions, respectively, in addition to a simple diffusion component (Materials and Methods). The corresponding relaxation time constants τ_n were on the nanosecond-to-microsecond timescale (Table 1).

We investigated the nature of these relaxations by a series of control experiments. (i) Relaxations were faster than the experimental diffusion time constant

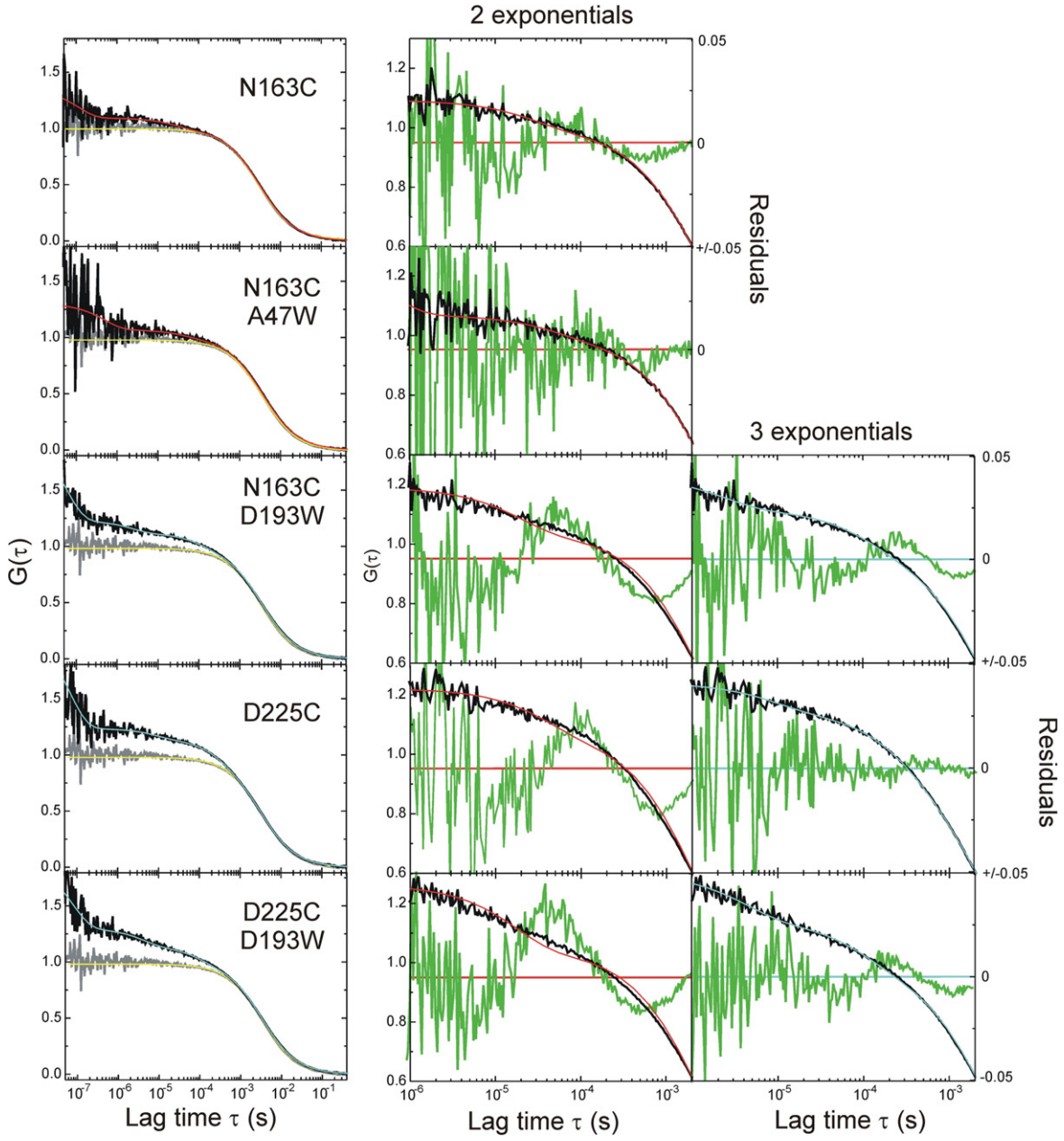

Fig. 4. FCS data analysis of AMPAR NTD. Left-hand column of panels: ACFs of all fluorescently modified NTD constructs as indicated (black data). The ACF of OVA is shown in gray for comparison, together with a fit to a model for a monodisperse diffusion without additional relaxations (yellow). NTD data are fitted to a model for a monodisperse diffusion with either two or three additional single-exponential relaxations (red or cyan lines, respectively). Middle- and right-hand columns of panels: close-ups of the microsecond time domain of NTD ACFs corresponding to the left-hand column of panels, with data fit to two- or three-exponential models (same color code as in left-hand column of panels). The residuals for each data fit are shown in green. The quality of fits can be judged by the randomness of the distributed residuals. Each ACF shown is normalized to the fitted average number of detected molecules *N* for reasons of clarity (see Materials and Methods).

of the free fluorophore of $\tau_D = \sim 600$ μs (Fig. 2c) and could therefore not arise from fluorophore contamination, which would give rise to the appearance of an additional decay with τ_D of the free fluorophore. (ii) Amplitudes and time constants of relaxations showed no significant excitation power dependence, demonstrating that they were not caused by photophysical effects intrinsic to the fluorophore (Supplementary Information, Fig. S1a). (iii) The number of molecules in the FCS detection focus scaled precisely with sample concentration in the picomolar-to-nanomolar range, and diffusion and relaxation time constants remained invariant (Fig. S1b and c), showing that possible concentration-dependent bimolecular interactions were not the origin of the observed fluctuations. Experiments (i) to (iii) ruled out nonstructural causes underlying the observed relaxations. Rather, it appeared that the sub-millisecond fluctuations were monomolecular and reported on protein conformational changes. In order to test more directly whether structural fluctuations were measured, we (iv) chemically reduced the native disulfide bond in the UL (C57–C309) by incubation of the sample with excess dithiothreitol (DTT). Removal of the disulfide bond led to a substantial increase in the amplitude and time constant of the observed microsecond relaxation, which is explained by the increased chain mobility within the perturbed protein (Fig. S1d). DTT itself did not give rise to additional fluorescence fluctuations caused by collisions of the agent with the fluorophore in solution, which was evident from experiments on a control protein lacking disulfide bonds (Fig. S1e). (v) The oxazine fluorophore showed significant modulation of its fluorescence quantum yield with changing solution polarity (Fig. S1f), demonstrating that the fluorophore reported polarity changes in its microenvironment, which may accompany structural changes in attached proteins. For example, tyrosine side chains can have some contribution to quenching of oxazine fluorescence.[33] From the results of experiments (i) to (v), we concluded that the sub-millisecond relaxations observed in the ACFs specifically reported structural fluctuations within the NTD.

Identifying specific motions in the AMPAR NTD

Trp side chains quench the fluorescence of oxazine labels *via* PET at van der Waals contact.[34] This selective fluorescence quenching, in combination with FCS, can be applied to detect ultrafast folding kinetics and segmental protein chain motions.[26,27] Recently, kinetics of helix motions have been uncovered successfully using this technique.[28]

We searched for motions along specific conformational coordinates in the AMPAR NTD using PET fluorescence quenching. Native Trp side chains (positions 124, 152, 256, 317, and 368) were structurally remote from the introduced labeling sites of the fluorophore (N163C and D225C; Fig. S2). We engineered a Trp side chain at sequence position 47 (A47W) in the UL into the background of N163C to probe a potential inter-lobe motion. Another Trp residue was placed at position 193 (D193W) in both mutant backgrounds N163C and D225C, respectively, to probe motions of helix G with respect to helix F and segment I, respectively (Fig. 3). In fact, these LL elements show variability when analyzing a series of AMPAR GluA2 NTD crystal structures[20] and feature higher *B*-factors when compared to the remainder of the protein (Fig. S3).

ACFs and FCS data analysis are shown in Fig. 4. The sub-millisecond relaxations of all NTD constructs fitted well to a model containing a sum of single-exponential decay functions besides a monodisperse diffusion. The number of relaxations required to obtain randomly distributed residuals varied with probe position. All FCS kinetic parameters extracted from data fits are summarized in Table 1. All constructs showed an ~100-ns relaxation that was difficult to quantify accurately due to the low signal-to-noise ratio in this time domain and the setup time resolution limit of ~40 ns. Two single-exponential relaxations were sufficient to describe the sub-millisecond decays of construct N163C-A47W, which were similar to N163C (Table 1). Therefore, no detectable inter-lobe motion between these positions was evident. Reporter construct N163C-D193W on helices F and G, on the other hand, showed an additional microsecond kinetic phase compared with construct N163C. This phase could, thus, be assigned to a specific motion of helix G relative to helix F, modulating formation and dissociation of fluorescence-quenching interactions between Trp193 and the fluorophore at C163 (Fig. 3). The kinetic phases of construct D225C, on the other hand, were not significantly affected by an engineered Trp side chain at position 193 (construct D225C-D193W; Fig. 4 and Table 1). The observed inter-element (helices F and G) and intra-element (segment I) dynamics in the LL occurred at locations that allow transmission of structural changes to downstream portions of the receptor, including the LBD (Fig. 1).

Discussion

Many cellular processes, such as enzyme catalysis or signal transduction, occur very rapidly on sub-millisecond timescales.[21] Associated protein conformational changes are often collective chain motions, that is, structural fluctuations between kinetically distinct states. The gating mechanisms of receptor channels emerge as complex multistep processes. In the case of acetylcholine receptors, for example,

gating is the sum of ultrafast allosteric communication between local structural changes spanning the entire length of the receptor, from the ligand-binding site to the pore helices.[35–37] Signal transmission is initiated by rapid localized movements of helices in response to ligand binding.[38]

FCS in combination with oxazine fluorophores extends the current spatial and temporal resolution limits of single-molecule spectroscopy and enables the direct observation of such elusive localized chain motions.[27,28] Here, we applied this technique to move into uncharted territory in the exploration of the energy landscape of the AMPAR GluA2 NTD.

The sub-millisecond relaxations in ACFs reported on kinetics of domain motions within the NTD. We avoided a microscopic interpretation of the observed kinetic quantities because a quantitative analysis of relaxation amplitudes was not possible: the amplitudes of sub-millisecond relaxations are a combination of the microscopic rate constants of interconversion of conformational states and the associated changes in fluorescence brightness of these states. The latter ones remained unknown. First, we analyzed relaxations of constructs that did not contain engineered Trp side chains, that is, N163C and D225C. While the sub-millisecond relaxation from sequence position 163 in helix F was little (construct N163C), the sum of relaxation amplitudes of the LL segment I (construct D225C) was ~3-fold higher (Table 1). In agreement with these findings, the comparison of available structural data sets of seven GluA2 NTDs (PDB IDs 3HSY, 2WJW, and 3H5V) shows significant displacements within the LL region (Fig. 5).[8,9,20] While the cores of structures fit to within an RMSD of 0. 5 Å, the LL helices F and G and segment I show marked variability with atomic displacements up to 10 Å.[20] In particular, segment I is the most variable of the three LL structural elements (RMSD of 3.2 Å over all backbone atoms) and adopts a largely disordered loop-like conformation. However, short α-helical stretches of one to two turns in segment I are apparent in some crystallographic data sets. By contrast, helix F is fully folded in the structures investigated, but missing all together in some data sets.[20] The pronounced nanosecond-to-microsecond relaxations detected in segment I might, therefore, originate from chain motions associated with formation of a nascent helix or helix–coil transitions. Indeed, isolated peptides fold into helices at ~500 ns.[39] The ~100-ns kinetic phases detected in all constructs, on the other hand, most likely reported very localized chain motions of loop segments comprising the labeling positions 163 and 225. Loop closure kinetics on similar timescales are observed in unfolded peptides and small protein domains,[27,32] while side-chain rotamers move on a faster picosecond-to-nanosecond timescale.[21]

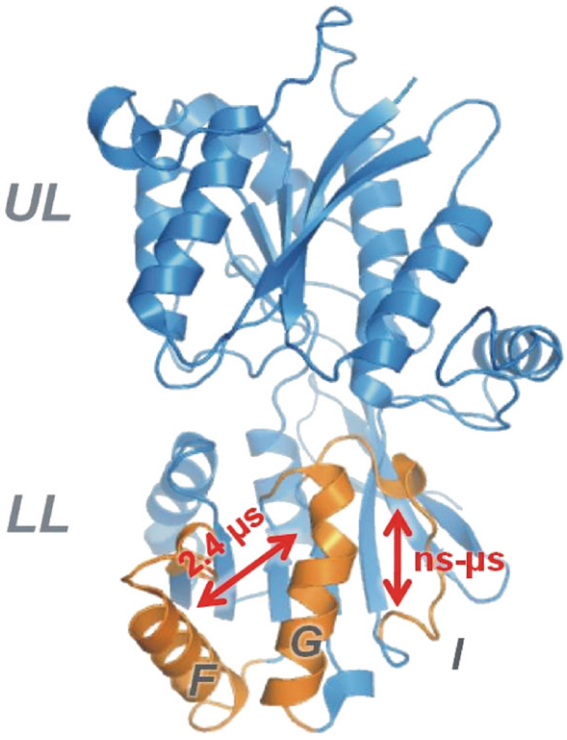

Fig. 5. Structural variability in AMPAR GluA2 NTDs. Chain segments that are found to be structurally variable from analysis of crystal structures with an RMSD up to 10 Å are highlighted orange (Ref. 20). Segments that superimpose with an RMSD <0.5 Å are highlighted blue. Chain motions and corresponding time constants identified by FCS are indicated by red arrows.

The comparative investigation of GluA2 NTD crystal structures reveals angular displacements of helices F and G of up to 47° and 21°, respectively.[20] Interestingly, the location of this structural heterogeneity coincides with the appearance of a 2.4-µs relaxation observed in PET–FCS experiments of a construct containing an engineered Trp side chain (N163C-D193W; Table 1 and Figs. 3 and 5). This relaxation might therefore well report on kinetics of motions of helices F and G with respect to each other. Hence, the relative displacements seen in various GluA2 NTD structures would consequently not originate from crystal artifacts but would rather reflect distinct conformational states on the free-energy landscape of the NTD, which are accessible and populated in solution. This interpretation is supported also by recent normal mode analysis.[20]

AMPA-type iGluRs activate and desensitize very rapidly on sub-millisecond timescales, transducing signals across synapses.[1,40] Consequently, the timescales of conformational changes triggering or modulating ion-channel gating have to be similar or faster. The nanosecond-to-microsecond motions

within the AMPA-type GluA2 NTD detected here by FCS fulfill this requirement.

The crystal structure of a full-length tetrameric AMPAR suggests extensive inter- and intra-subunit interactions of NTDs.[2,6] Chain segments in the LL of the NTD are in close vicinity to the semi-independent LBD located downstream in the receptor. Motions in the LL might well be part of an extended allosteric interaction network that transmits local conformational changes from the NTD to the LBD. A signaling capacity of the NTD could open new avenues for the design of effector compounds with pharmacological implications.

Materials and Methods

Expression of AMPA-type NTD and fluorescence modification

GluA2 NTD (Asn4–Glu391) with a glycosylation-reducing point mutation (N385Q) was subcloned into the pHLsec plasmid between a secretion signal sequence and a His_6 tag and was expressed in transiently and stably transfected GntI$^-$ HEK293S cells, as described previously.[41] Point mutations (N163C, A47W, D193W, and D225C) were introduced utilizing the QuikChange mutagenesis kit (Stratagene). Double mutants were made by using the same methodology. NTD secreted into the culture medium was purified to monodispersity by metal affinity and subsequent size-exclusion chromatography. Residues are numbered according to the mature polypeptide sequence.

Single Cys NTD point mutants were modified with the thiol-reactive maleimide derivative of the fluorophore AttoOxa11 (Atto-Tec). The excess fluorophore was added to the aqueous protein solution containing 50 mM potassium phosphate (pH 7.0), with the solution ionic strength adjusted to 200 mM using potassium chloride, and 2 mM tris(2-carboxyethyl)phosphine to prevent oxidation of the Cys side chain. The reaction was carried out for 2 h at 25 °C. The labeled protein was subsequently purified using size-exclusion chromatography on a Superdex 200 column (GE Healthcare) and using 50 mM potassium phosphate (pH 7.0) with 200 mM solution ionic strength as elution buffer. Under the employed reaction conditions, AttoOxa11 selectively targeted the solvent-exposed Cys side chain introduced by mutagenesis: control reactions under the same conditions using wild-type protein did not yield any detectable labeled protein.

Barnase, carbonic anhydrase, BSA, and OVA were modified at surface lysine side chains using the amino-reactive *N*-hydroxysuccinimidester derivative of the fluorophore Atto655, which has the same chromophore as AttoOxa11. Barnase was expressed as previously described,[42] and all other proteins were purchased from Sigma. Proteins were dissolved in 100 mM sodium carbonate (pH 8.0) and incubated with a 3-fold molar excess of amino-reactive fluorophore for 30 min at 25 °C. Labeled proteins were purified using size-exclusion chromatography on a Sephadex G-25 column (GE Healthcare). The average degree of labeling was 1.5 molecules of Atto655 per molecule of protein, as estimated by absorption spectroscopy.

FCS experiments and data analysis

FCS experiments were carried out on a home-built thermostatted confocal fluorescence microscope described elsewhere.[28] A laser excitation power of 400 μW at the back aperture of the objective lens was used throughout all experiments. This laser power was low enough to prevent photophysical artifacts in the ACFs. Labeled NTD was diluted to approximately 1 nM into buffered solution containing 50 mM potassium phosphate (pH 7.0), with the solution ionic strength adjusted to 200 mM using potassium chloride. We added 0.3 mg/ml BSA and 0.05% Tween-20 (both from Sigma) to the solution in order to diminish sample/glass-surface interactions. Solutions were filtered using a 0. 22-μm syringe filter prior to spectroscopy. FCS measurements on freely diffusing molecules were carried out at 25 °C in LabTek sample chambers (Nunc). The quartz glass surface of the chamber was passivated using poly-L-lysine prior to spectroscopy. To this end, the chamber was incubated with 10 mg/ml poly-L-lysine hydrobromide (Sigma) for 5 min at 25 °C and subsequently washed three times with buffer. ACFs of each sample were recorded for 30-min accumulated measurement time.

The second-order ACF is defined as:

$$G(\tau) = \frac{\langle I(t) \times I(t+\tau)\rangle}{\langle I(t)\rangle^2} \quad (1)$$

where $I(t)$ is the fluorescence intensity at time t, $I(t+\tau)$ is the fluorescence intensity after the time lag τ, and $\langle\rangle$ denotes the time average over the total observation time. Data were fit to a model[30] for a monodisperse diffusion in two dimensions containing either two or three additional single-exponential relaxations ($n=2$ or $n=3$):

$$G(\tau) = \frac{1}{N}\left(1+\frac{\tau}{\tau_D}\right)^{-1}\left(1+\sum_n a_n \exp\left(-\frac{\tau}{\tau_n}\right)\right) \quad (2)$$

where N is the average number of molecules in the detection focus, τ_D is the translational diffusion time constant, and a_n and τ_n are observed amplitude and time constant, respectively, of the nth relaxation. The two-dimensional model for translational diffusion is of sufficient accuracy for detection foci where the horizontal dimensions (x, y) are much smaller than the lateral (z) one, which was the case in the applied setup. All ACFs shown in figures were normalized to N for reasons of clarity.

Acknowledgements

M.H.J. was visiting master student from the University of Copenhagen (DK), Faculty of Pharmaceutical Sciences, Department of Medicinal Chemistry, and was supported by the Soransk Samfund (DK). M.S. is a member of the National Institutes of Health Cambridge Graduate Partnership Program and was funded by an Intramural Research Training Award from the National Institute of Child Health and Human Development (National Institutes of Health, USA). I.H.G. received

funding from the Royal Society (UK). M.H.J., M.S., C.M.J., I.H.G., and H.N. were supported by the Medical Research Council (UK).

Supplementary Data

Supplementary data to this article can be found online at doi:10.1016/j.jmb.2011.09.037

References

1. Traynelis, S. F., Wollmuth, L. P., McBain, C. J., Menniti, F. S., Vance, K. M., Ogden, K. K. *et al.* (2010). Glutamate receptor ion channels: structure, regulation, and function. *Pharmacol. Rev.* **62**, 405–496.
2. Sobolevsky, A. I., Rosconi, M. P. & Gouaux, E. (2009). X-ray structure, symmetry and mechanism of an AMPA-subtype glutamate receptor. *Nature*, **462**, 745–756.
3. Mayer, M. L. (2006). Glutamate receptors at atomic resolution. *Nature*, **440**, 456–462.
4. Oswald, R. E. (2007). Flexibility of a glutamate-binding domain. *Structure*, **15**, 1157–1158.
5. Soderling, T. R. & Derkach, V. A. (2000). Postsynaptic protein phosphorylation and LTP. *Trends Neurosci.* **23**, 75–80.
6. Hansen, K. B., Furukawa, H. & Traynelis, S. F. (2010). Control of assembly and function of glutamate receptors by the amino-terminal domain. *Mol. Pharmacol.* **78**, 535–549.
7. Rossmann, M., Sukumaran, M., Penn, A. C., Veprintsev, D. B., Babu, M. M. & Greger, I. H. (2011). Subunit-selective N-terminal domain associations organize the formation of AMPA receptor heteromers. *EMBO J.* **30**, 959–971.
8. Clayton, A., Siebold, C., Gilbert, R. J., Sutton, G. C., Harlos, K., McIlhinney, R. A. *et al.* (2009). Crystal structure of the GluR2 amino-terminal domain provides insights into the architecture and assembly of ionotropic glutamate receptors. *J. Mol. Biol.* **392**, 1125–1132.
9. Jin, R., Singh, S. K., Gu, S., Furukawa, H., Sobolevsky, A. I., Zhou, J. *et al.* (2009). Crystal structure and association behaviour of the GluR2 amino-terminal domain. *EMBO J.* **28**, 1812–1823.
10. Kumar, J., Schuck, P., Jin, R. & Mayer, M. L. (2009). The N-terminal domain of GluR6-subtype glutamate receptor ion channels. *Nat. Struct. Mol. Biol.* **16**, 631–638.
11. O'Hara, P. J., Sheppard, P. O., Thogersen, H., Venezia, D., Haldeman, B. A., McGrane, V. *et al.* (1993). The ligand-binding domain in metabotropic glutamate receptors is related to bacterial periplasmic binding proteins. *Neuron*, **11**, 41–52.
12. Quiocho, F. A. & Ledvina, P. S. (1996). Atomic structure and specificity of bacterial periplasmic receptors for active transport and chemotaxis: variation of common themes. *Mol. Microbiol.* **20**, 17–25.
13. Felder, C. B., Graul, R. C., Lee, A. Y., Merkle, H. P. & Sadee, W. (1999). The Venus flytrap of periplasmic binding proteins: an ancient protein module present in multiple drug receptors. *AAPS PharmSci.* **1**, E2.
14. Pin, J. P., Galvez, T. & Prezeau, L. (2003). Evolution, structure, and activation mechanism of family 3/C G-protein-coupled receptors. *Pharmacol. Ther.* **98**, 325–354.
15. Gielen, M., Siegler Retchless, B., Mony, L., Johnson, J. W. & Paoletti, P. (2009). Mechanism of differential control of NMDA receptor activity by NR2 subunits. *Nature*, **459**, 703–707.
16. Karakas, E., Simorowski, N. & Furukawa, H. (2009). Structure of the zinc-bound amino-terminal domain of the NMDA receptor NR2B subunit. *EMBO J.* **28**, 3910–3920.
17. Paoletti, P., Perin-Dureau, F., Fayyazuddin, A., Le Goff, A., Callebaut, I. & Neyton, J. (2000). Molecular organization of a zinc binding N-terminal modulatory domain in a NMDA receptor subunit. *Neuron*, **28**, 911–925.
18. Mony, L., Kew, J. N., Gunthorpe, M. J. & Paoletti, P. (2009). Allosteric modulators of NR2B-containing NMDA receptors: molecular mechanisms and therapeutic potential. *Br. J. Pharmacol.* **157**, 1301–1317.
19. Kumar, J. & Mayer, M. L. (2010). Crystal structures of the glutamate receptor ion channel GluK3 and GluK5 amino-terminal domains. *J. Mol. Biol.* **404**, 680–696.
20. Sukumaran, M., Rossmann, M., Shrivastava, I., Dutta, A., Bahar, I. & Greger, I. H. (2011). Dynamics and allosteric potential of the AMPA receptor N-terminal domain. *EMBO J.* **30**, 972–982.
21. Henzler-Wildman, K. & Kern, D. (2007). Dynamic personalities of proteins. *Nature*, **450**, 964–972.
22. Mittermaier, A. K. & Kay, L. E. (2009). Observing biological dynamics at atomic resolution using NMR. *Trends Biochem. Sci.* **34**, 601–611.
23. Palmer, A. G., III (2001). NMR probes of molecular dynamics: overview and comparison with other techniques. *Annu. Rev. Biophys. Biomol. Struct.* **30**, 129–155.
24. Kapanidis, A. N. & Strick, T. (2009). Biology, one molecule at a time. *Trends Biochem. Sci.* **34**, 234–243.
25. Schuler, B. & Eaton, W. A. (2008). Protein folding studied by single-molecule FRET. *Curr. Opin. Struct. Biol.* **18**, 16–26.
26. Neuweiler, H., Doose, S. & Sauer, M. (2005). A microscopic view of miniprotein folding: enhanced folding efficiency through formation of an intermediate. *Proc. Natl Acad. Sci. USA*, **102**, 16650–16655.
27. Neuweiler, H., Johnson, C. M. & Fersht, A. R. (2009). Direct observation of ultrafast folding and denatured state dynamics in single protein molecules. *Proc. Natl Acad. Sci. USA*, **106**, 18569–18574.
28. Neuweiler, H., Banachewicz, W. & Fersht, A. R. (2010). Kinetics of chain motions within a protein-folding intermediate. *Proc. Natl Acad. Sci. USA*, **107**, 22106–22110.
29. Hess, S. T., Huang, S., Heikal, A. A. & Webb, W. W. (2002). Biological and chemical applications of fluorescence correlation spectroscopy: a review. *Biochemistry*, **41**, 697–705.
30. Krichevsky, O. & Bonnet, G. (2002). Fluorescence correlation spectroscopy: the technique and its applications. *Rep. Prog. Phys.* **65**, 251–297.
31. Chattopadhyay, K., Saffarian, S., Elson, E. L. & Frieden, C. (2002). Measurement of microsecond dynamic motion in the intestinal fatty acid binding

protein by using fluorescence correlation spectroscopy. *Proc. Natl Acad. Sci. USA*, **99**, 14171–14176.
32. Teufel, D., Johnson, C. M., Lum, J. K. & Neuweiler, H. (2011). Backbone-driven collapse in unfolded protein chains. *J. Mol. Biol.* **409**, 250–262.
33. Marme, N., Knemeyer, J. P., Sauer, M. & Wolfrum, J. (2003). Inter- and intramolecular fluorescence quenching of organic dyes by tryptophan. *Bioconjug. Chem.* **14**, 1133–1139.
34. Neuweiler, H., Schulz, A., Boehmer, M., Enderlein, J. & Sauer, M. (2003). Measurement of submicrosecond intramolecular contact formation in peptides at the single-molecule level. *J. Am. Chem. Soc.* **125**, 5324–5330.
35. Auerbach, A. (2005). Gating of acetylcholine receptor channels: Brownian motion across a broad transition state. *Proc. Natl Acad. Sci. USA*, **102**, 1408–1412.
36. Purohit, P., Mitra, A. & Auerbach, A. (2007). A stepwise mechanism for acetylcholine receptor channel gating. *Nature*, **446**, 930–933.
37. Zheng, W. & Auerbach, A. (2011). Decrypting the sequence of structural events during the gating transition of pentameric ligand-gated ion channels based on an interpolated elastic network model. *PLoS Comput. Biol.* **7**, e1001046.
38. Unwin, N. (2003). Structure and action of the nicotinic acetylcholine receptor explored by electron microscopy. *FEBS Lett.* **555**, 91–95.
39. Kubelka, J., Hofrichter, J. & Eaton, W. A. (2004). The protein folding "speed limit". *Curr. Opin. Struct. Biol.* **14**, 76–88.
40. Erreger, K., Chen, P. E., Wyllie, D. J. & Traynelis, S. F. (2004). Glutamate receptor gating. *Crit. Rev. Neurobiol.* **16**, 187–224.
41. Aricescu, A. R., Lu, W. & Jones, E. Y. (2006). A time- and cost-efficient system for high-level protein production in mammalian cells. *Acta Crystallogr., Sect. D: Biol. Crystallogr.* **62**, 1243–1250.
42. Bycroft, M., Ludvigsen, S., Fersht, A. R. & Poulsen, F. M. (1991). Determination of the three-dimensional solution structure of barnase using nuclear magnetic resonance spectroscopy. *Biochemistry*, **30**, 8697–8701.